# TRANSONIC FLUTTER CONTROL OF A HIGH ASPECT RATIO WING : MATHEMATICAL MODELING, CONTROL LAW DESIGN AND WIND TUNNEL TESTS

Hiroshi MATSUSHITA, Masataka HASHIDATE, Kenichi SAITOH,
Yasukatsu ANDO, Kenji FUJII, Kouichi SUZUKI
National Aerospace Laboratory
Tokyo, Japan

and

Dario H. BALDELLI
Nagoya University
Nagoya, Japan

A promise and a limitation of a linear control for transonic limit-cycle flutter is investigated analytically, supported by wind tunnel test verification. A mathematical model simulating a transonic flutter of a wind tunnel aeroelastic model with control surfaces is derived by a linear structural and aerodynamic analysis. A finite element structural analysis and Doublet Point unsteady aerodynamic analysis, tuned by a ground vibration test and a wind tunnel flutter test, yield a math model which can predict experimental flutter characteristics with a certain discrepancy. Control laws with robust stability are synthesized based on the linear model and a control law attained experimentally 11.4% increase in the flutter dynamic pressure.

## Introduction

With the advent of modern high performance aerospace vehicles, interaction between structural dynamics, unsteady aerodynamics and control system has become prominent. Active control of aeroelastic system such as gust load response and flutter provides great benefit to vehicle safety, energy efficiency and flight performance for such a modern aircraft. Research efforts have been placed on establishing the relevant new technology, aeroservoelasticity, for more than two decades, and some of them have reached at a stage of practical use.

Recently Adams et al reported the capabilities and the application of their specific aeroservoelastic analysis tool named ISAC (Interaction of Structures, Aerodynamics, and Controls) system of program modules.[1] ISAC has been and is currently being used in many projects, among which NASA/Rockwell Active Flexible Wing (AFW) program has used it as a design tool and has succeeded in enhancing a flutter dynamic pressure by more than 23 %.[2]



On the other hand, National Aerospace Laboratory (NAL) has been carrying out experimental verification studies on active aeroelastic control and has developed a similar analytical procedure in low speed range.[3] The procedure has been successfully applied to active flutter control of a high aspect ratio wing.[4]

Owing to these research activities, aeroservoelastic analysis technology has reached at well establishing stage, at least in the subsonic speed range. It still remains, however, to extend the technology towards a transonic region where flutter dynamic pressure drops significantly, known as the transonic dip phenomenon. The present study aims at extending the technology to this transonic region, focusing on the establishment of an effective methodology for controlling nonlinear flutter.

## Transonic Flutter Wing Model and Test Devices

Japan Aircraft Development Corporation cooperated with kawasaki Heavy Industries investigated an aeroelastic characteristics of a supercritical wing.[5], [6] This aeroelastic wing model was refurbished to install a trailing edge and a leading edge control surface along with two sets of electric motors.

### Wing model design and construction

A plan form of the original wing model is similar and two third of our low speed wind tunnel model. The model simulates a high aspect ratio wing of advanced energy efficient aircraft.

Refurbishing items are to provide control surfaces with their activating motors, accelerometers on the wing and a computer for a feedback purpose. Trailing edge and leading edge control surfaces were designed as the same geometric shape and position as

its low speed counterpart; hinge lines are at 73% and 15% chord position and both surfaces range from 62.6% to 80.9% span position. Hinge moment of the control surface were estimated to need 294 Nm torque for an actuator so that a brushless DC servo-motor of 30 W rated output, with reduction gear of sixtieth ratio, was selected. Since the volume of these geared motors are too large to be accommodated within the original cross section of the wing, it was decided to reform the section of the mid wing from original supercritical wing to symmetrical NACA airfoil, keeping the thickness ratio the same as the original wing. For maintenance purpose, this portion are divided into five parts, made by FRP, and each section is attached to a spar by screws along the elastic axis which is similar to a pod configuration typical for a low speed aeroelastic model. A geometry of a refurbished model wing is shown in Fig. 1.

Flutter stopper development

Since the wind tunnel study in the low speed range revealed that a flutter stopping device is a very powerful tool for carrying out tests efficiently by preventing models from being destroyed by flutter, the device was developed for use at a transonic wind tunnel.

A cost effective device was examined by modifying the flutter stopper of "NAL method" for a low speed wind tunnel[7],[8]. Instead of a wire net method intending the flow speed deceleration used at a low speed wind tunnel, an effect of changing the cross section area with bypass to the plenum chamber was considered. Due to the ease of installation and according to the results of scaled model tests, the device is installed at the opposite side of the model. In this configuration, the wake from the plate itself does not cover the flutter model. The set up of the device installed in the transonic wind tunnel test section with a flutter model wing is shown in the Fig. 2. Ordinarily the plate is laid flat on the test section floor. When a wing goes into flutter, it is engaged instantaneously to protrude in the stream.

Fig. 3 shows the measured results where decreased dynamic pressure due to flutter stopper activation are depicted against a free stream Mach number for different reservoir pressure $P_0$ of the wind tunnel. The dynamic pressure decrement is remarkable; for instance, at Mach 0.8 and 100 KPa of $P_0$, 29.4 KPa dynamic pressure decreases by 8.6 KPa which corresponds to 29.6 % decrease. The dynamic pressure decrement at another Mach number and $P_0$ reaches well over 28 % and the corresponding Mach number decrement is over 20 %. The device was used in transonic flutter control tests 30 times and was able to prevent a wing model from being destroyed by flutter. The time chart of the effectiveness of this device will be shown at the latter section.

Mathematical Modeling

In order to proceed synthesizing a control law for active flutter suppression, the first step is to derive a mathematical expression for a controlling plant. In transonic range, strength of a shock wave is very sensitive to pressure gradient around a wing, and, in case of unsteady situation, is dependent on the amplitude of oscillation. Transonic flutter, therefore, often behaves like nonlinear and is difficult to be expressed with a simple linear mathematical formulation. Reserving a more sophisticated transonic codes like a transonic small disturbance code for future investigation, however, the present study intends to investigate a potential applicability of a robust control design method under these circumstances with uncertainty.

In this section we derive a linear mathematical model for this wind tunnel wing model by almost the same manner as for the low speed flutter suppression. Subsonic lifting surface method of Doublet Point is adopted for analyzing unsteady aerodynamics.

With an expression of a flexible wing deformation $z(x,y,t)$ by $N$ structural modes, $z_{qi}(x,y)$, and two control surface modes $z_{\delta j}(x,y)$ such as

$$z(x,y,t) = \sum_{i=1}^{N} z_{qi}(x,y)q_i(t) + \sum_{j=1}^{2} z_{\delta j}(x,y)\delta_j(t) \qquad (1)$$

fundamental equations for aeroelastic wing is expressed as[9],[10].

$$\boldsymbol{M}\ddot{\boldsymbol{q}} + \boldsymbol{B_c}\dot{\boldsymbol{q}} + \boldsymbol{K}\boldsymbol{q} + \boldsymbol{S}\ddot{\delta} = \boldsymbol{f_a} \qquad (2)$$

In eq.(1), $q_i(t)$ and $\delta_j(t)$ are the generalized coordinates and control surface deflection, respectively. Mass matrix $\boldsymbol{M}$, damping matrix $\boldsymbol{B_c}$ and stiffness matrix $\boldsymbol{K}$ have the following elements,

$$\boldsymbol{M} = diag(m_1, m_2, \ldots, m_N) \qquad (3a)$$

$$\boldsymbol{B_c} = diag(2m_1\zeta_1\omega_1, 2m_2\zeta_2\omega_2, \ldots, 2m_N\zeta_N\omega_N) \qquad (3b)$$

$$\boldsymbol{K} = diag(m_1\omega_1^2, m_2\omega_2^2, \ldots, m_N\omega_N^2) \qquad (3c)$$

$$\boldsymbol{S} = \{ s_{ij} \} \qquad (3d)$$

In these element, the generalized masses have the expression as,

$$m_i = \iint_S z_{qi}^2(x,y)\rho(x,y)dxdy \qquad (3e)$$

and $\zeta_i$ and $\omega_i$ are i-th structural mode frequency and its damping. The last term on the left hand side of Eq.(2) is an inertial coupling term; $s_{ij}$ represents the inertial force coefficient on the i-th mode due to j-th

control surface activity. The terms $f_a$ on the right hand side of Eq.(2) are generalized aerodynamic forces due to aircraft motion. They can formally be expressed by generalized coordinates and aerodynamic influence matrix $F_a(k,M)$ as,

$$f_a = F_a(k,M)\, q \tag{4a}$$

and the elements of $F_a(k,M) = \{ f_{aij} \}$ are defined by the pressure distribution caused by aircraft motion $\Delta p_a(x,y;k,M)$ such that

$$f_{aij} = \iint_S \Delta p_{aj}(x,y;k,M)\, z_{qi}(x,y) dxdy \tag{4b}$$

The pressure distributions in Eq. (4b) are determined for each Mach number $M$ and reduced frequency $k=bw/U$; $b$, $w$, $U$ being a half mean aerodynamic chord, circular frequency and flow velocity. First, mode shapes $z_{qi}(x,y)$ have to be determined, then generalized aerodynamic forces $f_{aij}$ are analyzed.

Structural math model tuned by ground vibration test

Vibration test of a refurbished model was carried out.[11] The wing was vibrated at an appropriate single point and deflections at 39 points over the wing surface were measured by a laser deflection meter. Data were analyzed by modal analysis software and obtained modal parameters such as natural frequency, damping and mode shape. Fig. 4 shows the nodal line where the first four vibration modes are depicted for two different vibration methods: random vibration and sine dwell. Rigidity of the wing was also measured.

Based on these vibration test results, a structural math model was constructed. By adjusting the analytical natural frequencies and modes to measured data, mass and rigidity distribution are tailored until analysis and measurement coincide with each other. Resulting modal parameters are listed in Table 1. Frequencies of the first four modes which will play an essential role in flutter are estimated very good within 3% error. Structural math model yields modal lines as shown in Fig. 5 and shows good agreement with the measured results as shown in Fig. 4. The good correspondence of mode shape is shown more intuitively in Fig. 6 for a typical mode of first torsion.

Finite dimensional aerodynamic model

Using the vibration modes obtained, unsteady aerodynamic analysis was carried out by Doublet Point method. The asterisk in Fig. 7 shows the analytical results of generalized unsteady aerodynamic forces for the first four modes caused by their own mode oscillation and by two control surface activation at eleven different reduced frequencies. Flow Mach number is the design Mach number of 0.8.

The generalized aerodynamic forces Eq. (4a) are distributed infinite dimensional system in its nature; they are governed by partial differential equations. In order to apply the optimal control theory, it is necessary to approximate them with a lumped parameter finite dimensional system. The resulting expression may be expressed by the first order lag system using the supplementary variables $r$ such as,

$$f_a(t) = A_2 (\ddot{q}(t)^T \ddot{\delta}(t)^T)^T + A_1 (\dot{q}(t)^T \dot{\delta}(t)^T)^T + A_0 (q(t)^T \delta(t)^T)^T + r(t) \tag{5a}$$

$$\dot{r}(t) = \Lambda r(t) + B_0 (q(t)^T \delta(t)^T)^T \tag{5b}$$

where $\Lambda = diag(-\lambda, \ldots, -\lambda)$

$A$-matrices in the above equations represent the quasi-steady nature of the airload, while the supplementary variables $r$ expresses the phase delay nature essential to unsteady flows. The methods of obtaining the coefficients of the matrices in these equations have been investigated by many researchers. The present synthesis procedure adopts a method in the frequency domain by Roger[12]. The data shown by asterisks in Fig. 7 were fitted by linear system of Eq. (5) in minimum least square sense and the results are shown as the solid lines. It should be noted that approximation is almost good except the last column of a trailing edge contribution, where the fitting in the second and the third mode generalized aerodynamics are poor.

Finite state aeroelastic model

Each of the control surface activating systems has a band width of 40 Hz at 1 deg. deflection amplitude. In the fundamental equations are included their dynamics which can be described by the second order system as

$$\ddot{\delta} + C_\delta \dot{\delta} + K_\delta \delta = K_\delta \delta_c \tag{6}$$

where $C_\delta = diag(2\zeta_{\delta 1}\omega_{\delta 1}, 2\zeta_{\delta 2}\omega_{\delta 2})$ (7a)

$$K_\delta = diag(\omega_{\delta 1}^2, \omega_{\delta 2}^2) \tag{7b}$$

and control command :

$$\delta_c = (\delta_{c1}, \delta_{c2})^T \tag{7c}$$

The Eq. (2) with Eqs. (5a) and (5b) along with the control equation (6) constitutes the fundamental equations for an aeroelastic wing with controls.

With a state variable vector defined as $x = (\dot{q}^T, \delta^T, q^T, \delta^T, r^T, w_g)^T$, the governing equations are eventually

written in the form of a state space model as

$$\dot{x}(t) = Ax(t) + Bu(t) + w(t) \tag{8}$$

Components of $u$ are the control commands. A system noise $w$ introduced at the right hand side of the equation represents some noise source and is a white noise. An order of the math model amounts to sixteen.

The observable output which can be used for feedback signal, such as accelerometer, wing spar strain, etc, can be expressed by the state and control variables as

$$y(t) = Cx(t) + Du(t) + v(t) \tag{9}$$

with $v$ being a measurement noise.

Now that the elements of the aerodynamic influence matrix are calculated, flutter characteristics of the wing can be estimated using Eq. (8). The finite dimensional math model can therefore be checked by comparing the flutter characteristics obtained by analysis and wind tunnel tests.

Flutter test and model tuning

The original wing had specific transonic flutter features of transonic dip and of limit cycle. The present refurbishment, particularly adding a mass of motors and their cover pods and changing a wing shape at the portion of the pods, may have modified the flutter characteristics. The wind tunnel flutter tests were therefore planed and conducted to confirm the change in flutter characteristics stressing particularly the transonic dip phenomena and the limit cycle nature. The test results are shown in Fig. 8(a) as a flutter dynamic pressure versus Mach number and in Fig. 9 as time histories of acceleration response. It can be seen in these figures that the present wing remains the same characteristics of a transonic dip and a limit cycle nature as the original wing. Due to increasing mass the flutter frequency is lowered to around 20 Hz from the original wing frequency of over 40 Hz though. It is noted that the amplitude of a limit cycle flutter increases with a flutter dynamic pressure; at the bottom of a dip, flutter is rather mild.

In each time history, a limit cycle flutter were ceased by activating a flutter stopper. When the device is engaged, the amplitude of flutter turns to decrease within few cycles of oscillation. The effect of this device is depicted in Fig. 8(b) where it can be seen that the device decreases Mach number and dynamic pressure by over 30 % along a constant $P_0$ line.

Comparing these experimental values for flutter, it turned out that the analytical results predicted too lower the flutter dynamic pressure. A reduction factor had to be introduced to multiply a calculated aerodynamic forces. The reduction factor was determined so as to minimize the deference between experimental and estimated flutter dynamic pressure in the range of transonic dip phenomena. The reduction factor thus obtained is as less as 0.368. The root locus were obtained for the tuned math model and is shown in Fig. 10. The estimated flutter boundary is depicted along with the experimental data in Fig. 8(a).

## Control Law Synthesis and Wind Tunnel Test Verification

Control laws for active flutter suppression are synthesized based on the math model which was induced in the previous section. As can be seen in Fig. 3.4a, the math model does not satisfactorily represent a real flutter characteristics. It was decided to design a control law with robust stability nature against a math model insufficiency. For the purpose of comparison, the LQG synthesis was also tried.

The design specification was determined to extend the open loop flutter dynamic pressure at Mach 0.8 by 20 % within an allowable control surface activation of 1 deg deflection and 90 deg/sec angular velocity. Furthermore, in the case of robust design, the specification should be satisfied against ±10 % deviation of aeroelastic parameters of the first and second mode stiffness which have the critical effect to plant stability. In the following section, these two synthesis methods are briefly described.

LQG control synthesis

For flutter control, the performance index can be defined by the system kinetic energy plus control cost as follows,

$$J = \mathrm{E}\{\tfrac{1}{2}x^TQx + \tfrac{1}{2}u^TRu\} \tag{10}$$

Since the state equation, the output equation and the performance index are obtained in the standard form of the optimal output regulator problem, the full-order output feedback control law can be derived as a combination of a regulator and Kalman estimator as follows[13]. First, the state feedback optimal regulator part can be expressed using an estimated state as,

$$u = -K_1\hat{x} \tag{11}$$

where the optimal gain $K_1$ is given as,

$$K_1 = R^{-1}B^TP_1 \tag{12}$$

and $P_1$ is the solution to the following matrix Riccati equation.

$$A^TP_1 + P_1A - P_1BR^{-1}B^TP_1 + Q = 0 \tag{13}$$

As a state observer, the present synthesis method utilizes Kalman estimator; the dynamics of the estimator have the following formula.

$$\dot{\hat{x}} = A\hat{x} + Bu + K_2 (y - C\hat{x} - Du) \quad (14)$$

where the Kalman gain $K_2$ is given by another Riccati equation such as,

$$AP_2 + P_2A^T - P_2C^TV^{-1}CP_2 + W = 0 \quad (15)$$

$$K_2 = P_2C^TV^{-1} \quad (16)$$

The order of this output feedback controller is the same as the plant. Since a full order controller has in general too high an order to be implemented in an on-board computer in real time sense, order reduction is necessary. Furthermore, there might be some state variables in the control law which make a lesser contribution to the control performance. Using the order reduction method of a residualization and a balanced truncation approximation, we can finally obtain the following reduced order output feedback control law.

$$\dot{z} = Fz + Gy \quad (17a)$$

$$u = Hz \quad (17b)$$

Control laws of flutter control for the present model were synthesized by these LQG method and an estimated control performance for a typical candidate for wind tunnel test is listed at the first column in Table 2. In order to be free from aliasing problem for signal sampling of 500 Hz, anti-aliasing filter of 100 Hz is inserted prior to A/D converter. As can be seen in the table, this control law is estimated to increase a flutter dynamic pressure by 29.3% at least at the nominal condition.

Robust stability control synthesis

Robust stability control design based on coprime factors approach was applied to this wing model and the reduced order controller was obtained by the residualization method which yielded control laws with a certain level of robustness.[14] The design process combines classical open-loop shaping principle with an $H_\infty$ robust stabilization problem in the normalized coprime factors framework. The detailed process is stated in Reference 14.

Let the nominal plant model $G(s)$ have a normalized left coprime factorization such as,

$$G(s)=M(s)^{-1}N(s)$$

where $N(s)N(s)^* + M(s)M(s)^* = I$ for all s, and $N(s)$, $M(s)$ are asymptotically stable proper real rational functions and $M(s)^* = M(-s)^T$. The uncertainties in the plant can be represented in terms of additive stable perturbations $[\Delta N(s), \Delta M(s)]$ to the factors in a coprime factorization of the plant as shown in Fig. 11.

Let a minimal realization of a proper plant be $G(s) = (A, B, C, D)$, and let $X, Z > 0$ be the positive definite solution to the algebraic Riccati solutions

$$A_X^*X + XA_X - XBS^{-1}B^*X + C^*R^{-1}C = 0 \quad (19)$$

$$A_ZZ + ZA_Z^* - ZC^*R^{-1}CZ + BS^{-1}B^* = 0 \quad (20)$$

where $A_X$ and $A_Z$ are

$$A_X = A - BS^{-1}D^*C$$

$$A_Z = A - BD^*R^{-1}C$$

then, for a given $0 < \varepsilon < \varepsilon_{max}$, the state space realization of a central controller $K_\phi$ is given, using Doyle's notation, as

$$K_\phi(s) = \left[\begin{array}{c|c} A^c + e^{-2}W_1^{-1}ZC^*(C+DF) & e^{-2}W_1^{-1}ZC^* \\ \hline B^*X & -D^* \end{array}\right] \quad (21)$$

$$S = I + D^*D, \quad R = I + DD^*, \quad A^C = A + BF$$
$$W_1 = I + (XZ - \varepsilon^{-2}I), \quad F = -S^{-1}(D^*C + B^*X)$$

The maximum stability margin, $\varepsilon_{max}$, is given as

$$\varepsilon_{max} = [\, I + \lambda_{max}(ZX) \,]^{-1/2} \quad (22)$$

where $\lambda_{max}(ZX)$ is a maximum Hankel norm for the nominal plant and is a function of ZX.

In order to incorporate performance objectives, the normal plant is extended with input and output shaping functions $W_i(s)$, $W_o(s)$. The extended plant is given as $G_e(s) = W_oGW_i(s)$ and feedback controller is given as

$$K_e(s) = W_iK_\phi W_0(s) \quad (23)$$

where a controller $K_\phi$ is obtained from Eq. (22) by substituting a plant dynamics $G(s)$ with $G_e(s) = (A_e, B_e, C_e, D_e)$. The maximum stability margin for an extended plant can be expressed accordingly as

$$\varepsilon_{emax} = [\, I + \lambda_{max}(Z_eX_e) \,]^{-1/2} \quad (24)$$

To this control law, order reduction method is applied. Reduction process is divided into two steps; the first step is to reduce a plant order itself by a residualization method and the second step is to reduce

a control law order by a residualization with a balanced truncation approximation process.[14]

Control laws were synthesized by these procedure supported by a physical simulation; a control law was checked and refined, if necessary, by implementing in a computer, setting up all the devices and engaging a system in a closed loop state. Since the structures like an aeroelastic system have lots of modes successively aligned, frequency shaping may have an effective benefit to prevent an instability caused by spill-over or model error. Different kinds of shaping functions were therefore investigated. The filter frequency was reduced to 75 Hz since the control law C1 was revealed instable when 100 Hz filter was applied. The second law in Table 4.2a shows its results. Though the order of 6 is little bit high for implementing it to computer, the predicted closed loop flutter dynamic pressure is almost doubled over the open loop value.

Aiming at preventing instability by reducing a gain at higher frequency than the third mode, low pass filter and a notch filter were applied as a shaping function. Three different control laws were designed. In Table 2, C2 is an original control law and C3 is revised it in increasing a gain at a low frequency region and decreasing at a high frequency. C3 is to moderate these gain modification.

In a typical case of control law C2, the robustness in stability were checked by changing two important aeroelastic parameters, the first and the second mode stiffness. Table 3 shows the sensitivity of closed-loop flutter dynamics pressure due to parameter perturbations. As can be seen in this table, though the decrement in the second mode frequency has a serious effect to decrease a flutter dynamic pressure, control law C2 still maintains a stability margin at an open-loop flutter boundary of an estimated dynamic pressure of 23.89 KPa.

## Flutter control wind tunnel test

In order to estimate a practical performance of the control laws designed, wind tunnel tests were performed. A block diagram of the wind tunnel test is shown in Fig. 12. A control law is installed in the digital computer which processes an input signal from an accelerometer to produce an output feedback signal to a control surface actuating motor. As the flutter tests were proceeded, it was found out that the flutter dynamic pressure decreased gradually when the wing experienced a flutter; a severe flutter vibration might decrease the binding strength of the screw of the wing pods. The uncontrolled flutter condition was therefore confirmed just before each controlled test.

In the test, at a subcritical speed the loop is closed, and after making sure that there is no unexpected problem, the wind tunnel dynamic pressure is increased gradually until a closed loop system goes unstable.

## Results and discussion

The test results for five control laws are listed in Table 2. When C1 control law was cast into wind tunnel test, it experienced instability due to third mode excitation. It was decided to halve its control gain. The experimental values in Table 2 is those at this gain value.

As a typical test result a time history of a control surface activation and an acceleration for control law C2 is shown in Fig. 13. When the system is engaged, acceleration response can be seen to be suppressed at a low frequency of around 20 Hz. Fig. 14 shows this change more clearly that the level of the lowest mode is decreased by almost ten dB and the damping of this mode increases. These effect results in the increment of 11.4 % in the flutter dynamic pressure.

As can be seen in Table 3 all the increment of flutter dynamic pressure attained in the tests are almost third of the estimated values. Two statements are drawn from the results; first, it can be stated that the robust stability method is validated its effectiveness since the method succeeded in increasing a flutter boundary in the situation that the math model based is a linearized model and has a certain level of discrepancy to a nonlinear transonic flutter phenomena.

It should also be mentioned that, since the difference between the predicted values and the test results are not small, the research effort to take a transonic code into math modeling procedure should be made in order to improve the math model. In this respect, Batina et al tried to apply transonic codes to aeroelastic modeling and investigate possible flutter speed increment with a simple feedback control.[15] They showed that almost the same procedure applied to subsonic region can also be applied to a transonic region. Their method should be extended to a more elaborate control problem. According to the intensive research efforts conducted worldwide in recent years, transonic aeroelastic behavior of an aircraft, even with a control surface, can now be simulated with satisfactory precision; which constitutes a firm basis for developing a transonic aeroservoelastic system design.

Another direction of future research for improving the control effectiveness is to use a leading edge control surface. The successful results using a leading edge surface for flutter control in a low speed range at NAL[16] suggests a promise in a transonic range as well.

## Conclusions

A promise and a limitation of a linear control for transonic limit-cycle flutter is investigated analytically, supported by wind tunnel test verification.

The effectiveness of the robust stability method is validated. Though the math model is a linearized model and has a certain level of discrepancy to a nonlinear transonic flutter phenomena, the control law designed by the method succeeded in increasing a flutter boundary by 11.4 % of dynamic pressure.

The difference between the predicted values and the test results are not small, however, the research effort to take a transonic code into math modeling procedure have to be taken in order to improve the math model.

## Reference


1. Adams, W. M., Jr. and Tiffany, S. H., "ISAC: A Tool for Aeroservoelastic Modeling and Analysis." AIAA Paper 93-1421-CP, Presented at the 34th Structures, Structural Dynamics and Materials Conference, 1993.
2. Perry, B., III, Cole, S. R., and Miller, G. D., AIAA-92-2080-CP, and many other papers appearing in the Proceedings of 1992 AIAA Dynamics Specialists Meeting.
3. Matsushita, H., Fujii, K. and Miyazawa, Y., "Active Aeroelastic Control of an Aircraft: Control Law Synthesis and Wind Tunnel Test Verification," The Proceedings of the 1st International Conference on Motion and Vibration Control (MOVIC), Yokohama, Japan, pp.706-711.
4. Ueda, T., Matsushita, H., Suzuki, S. Miyazawa, Y. and Matsuzaki, Y., "ACT Wind-Tunnel Experiment of a Transport-Type Wing," *J. Aircraft*, 28-2(1991), pp.139-145.
5. Yonemoto, K., "A Practical Method for Predicting Transonic Wing Flutter Phenomena," ICAS 84-1.7.1, Sept. 1984.
6. Yonemoto, K., Akatsuka, T., Hiraoka, K. and Mito, S., "Transonic Flutter Calculation Method and Wind Tunnel Test Study of High Aspect Ratio Wing," KHI Technical Report, No. 105, 1990, in Japanese.
7. Hanzawa, A., et al, "Preliminary Tests of a Flutter Emergency Stopper for the Transonic Wind Tunnel - (Part 1) Basic Performance Tests for Flutter Stopper", NAL TR-1197, 1993, in Japanese.
8. Ando, Y., et al, "Preliminary Tests of a Flutter Emergency Stopper for the Transonic Wind Tunnel - (Part 2) Detailed Study for Flutter Stopper Development", NAL TR-1200, 1993, in Japanese.
9. ACT Study Group, "Gust Load Alleviation of a Cantilevered Rectangular Elastic Wing. — Wind Tunnel Experiment and Analysis," NAL TR-846, 1984, in Japanese.
10. Bisplinghoff, R. L., Ashley, H. and Halfman, R. L., *Aeroelasticity*, Addison-Wesley Publishing Co., 1955.
11. Fujii, K., et al, "Preliminary Tests of a Transonic Flutter Control Wing Model," The Proceedings of the 30th JSASS Aircraft Symposium, Tsukuba, Japan, 1992, pp.474-477, in Japanese.
12. Roger, K. L., "Airplane Math Modeling Method for Active Control Design," AGARD-CP-228, 1977, pp.4.1-11.
13. Kwakernaak, H. and Sivan, R., *Linear Optimal Control Systems*, Wiley-Interscience(1972).
14. Baldelli, D. H., Ohta, H. and Matsushita, H., "Robust Stabilization of an Aeroelastic Wing Model using Normalized Coprime Factors Approach," The Proceedings of the 31st JSASS Aircraft Symposium, Tokyo, 1993, pp.74-77.
15. Batina, J. T. and Yang, T. Y., "Application of Transonic Codes to Aeroelastic Modeling of Airfoils Including Active Controls," Journal of Aircraft, Vol. 21, No. 8, 1984, pp. 623-630.
16. Matsushita, H., Miyazawa, Y., Ueda, T. and Suzuki, S., "Multi-Surface Control Law Synthesis and Wind Tunnel Test Verification of Active Flutter Suppression for a Transport-Type Wing," The proceedings of the European Forum on Aeroelasticity and Structural Dynamics, Aachen, FRG, 1989, pp.519-527.


Table 1 Natural frequency of the wing model

[Hz]

| Natural Mode | GVT Random | GVT Sine | Math Model |
|---|---|---|---|
| 1st Bending | 12.5 | 12.22 | 12.52 |
| 2nd Bending | 37.0 | 37.23 | 36.23 |
| 1st Torsion | 44.0 | 45.11 | 44.01 |
| 3rd Bending | 86.5 | 87.20 | 90.10 |
| 2nd Torsion | 134.0 | 134.64 | 138.06 |
| 4th Bending | 173.0 | 177.33 | 172.45 |

Table 2 Control law performance

| Ctrl Law | Ordr | ANF[a] [Hz] | Shaping Function Gain | LPF[b] [Hz] | NTF[c] [Hz] | Analysis $q_{OL}$ [Kpa] | Analysis $q_{CL}$ [Kpa] | Analysis [%] | Experiment $q_{OL}$ [Kpa] | Experiment $q_{CL}$ [Kpa] | Experiment [%] |
|---|---|---|---|---|---|---|---|---|---|---|---|
| Q1[d] | 4 | 100 | — | — | — | 23.00 | 29.75 | 29.3 | 21.43 | 23.56 | 9.9 |
| C1[e] | 6 | 75 | 5 | — | — | 23.59 | 46.32 | 96.4 | 21.78 | 24.20 | 11.1 |
| C2[e] | 4 | 75 | 2 | 35 | 40 | 23.89 | 32.40 | 35.6 | 26.68 | 29.72 | 11.4 |
| C3[e] | 4 | 75 | 5 | 30 | 40 | 23.89 | 36.77 | 53.9 | 26.68 | 29.13 | 9.2 |
| C4[e] | 4 | 75 | 3 | 30 | 40 | 23.89 | 33.83 | 41.6 | 25.55 | 28.35 | 11.0 |

a)ANF:Anti-Aliasing Filter, b)LPF:Low Pass Filter, b)NTF:Notch Filter
d) LQG, e) Normalized Coprime Factors Approach

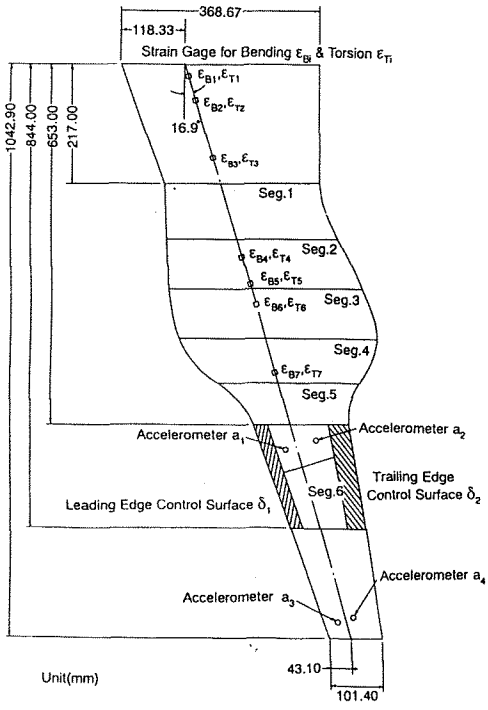


Fig. 1 Aeroelastic wing model for flutter control

Table 3 The sensitivity of closed-loop flutter dynamic pressure due to parameter perturbations

| $\omega_1$ ⋱ $\omega_2$ | -10% | Nom. | +10% |
|---|---|---|---|
| -10% | 25.74 | 33.11 | 42.21 |
| Nom. | 25.12 | 32.40 | 42.21 |
| +10% | 24.50 | 31.70 | 42.21 |

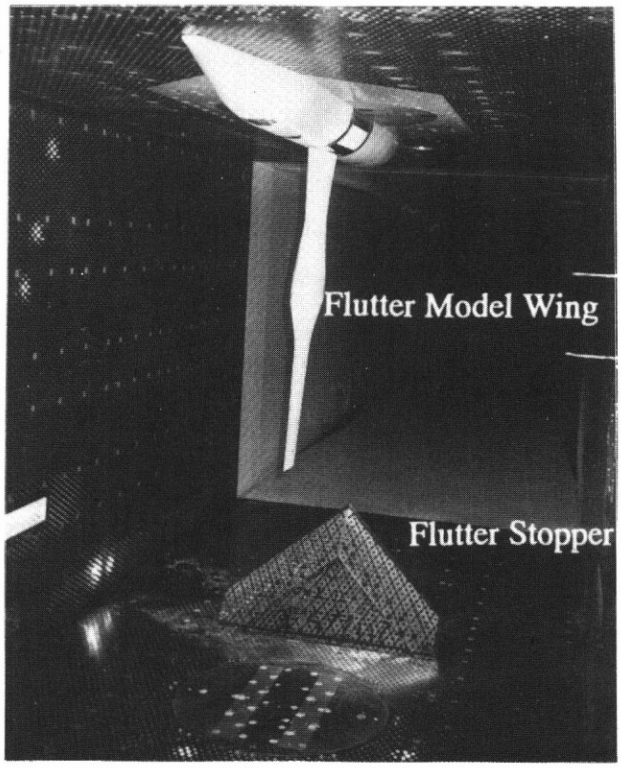


Fig. 2 Transonic flutter wind tunnel set-up showing a model and a flutter stopper

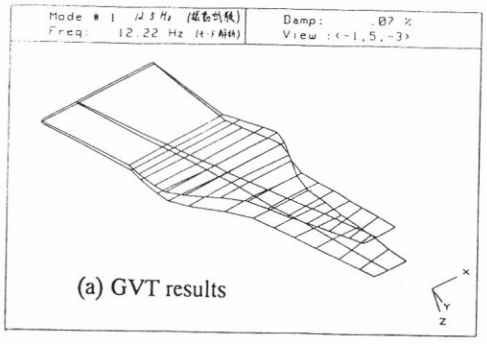


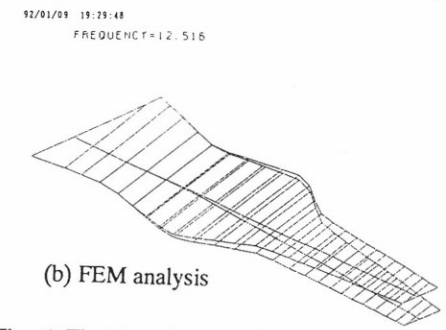


Fig. 6 First torsion mode shape of the wing

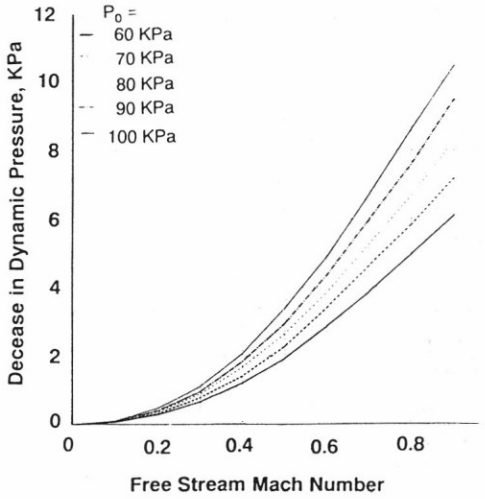


Fig. 3 Decrease in dynamic pressure and Mach number due to the flutter stopper

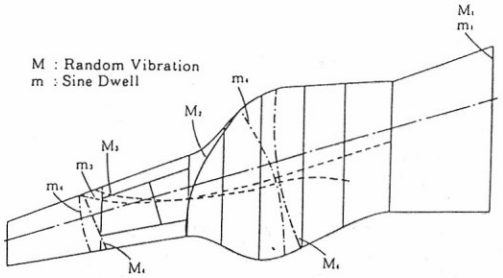


Fig. 4 Nodal line measured in GVT

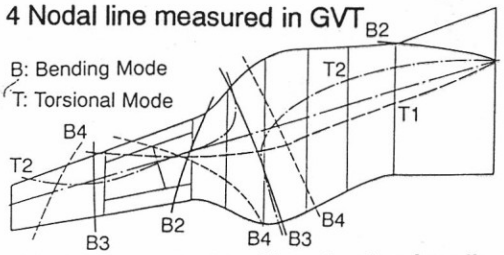


Fig. 5 Nodal line calculated by structural math model

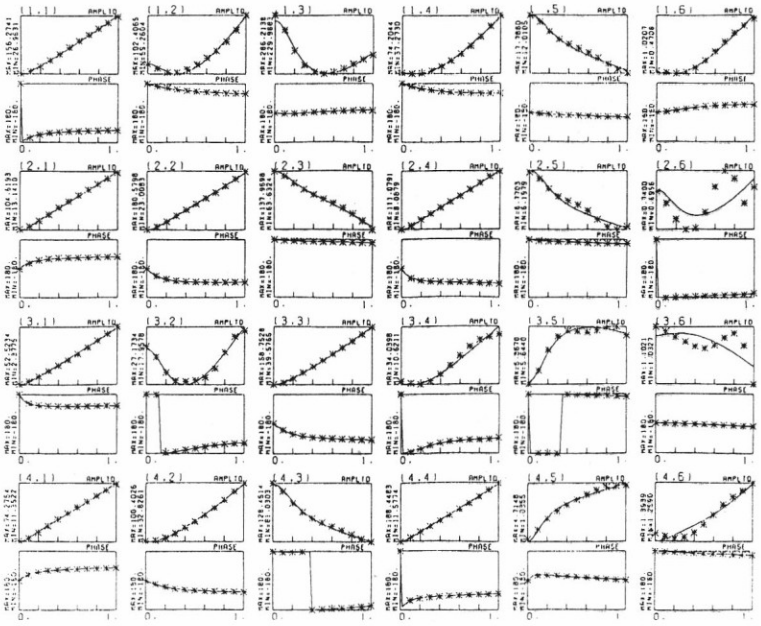

Fig. 7 Finite state fitting of the generalized aerodynamic forces

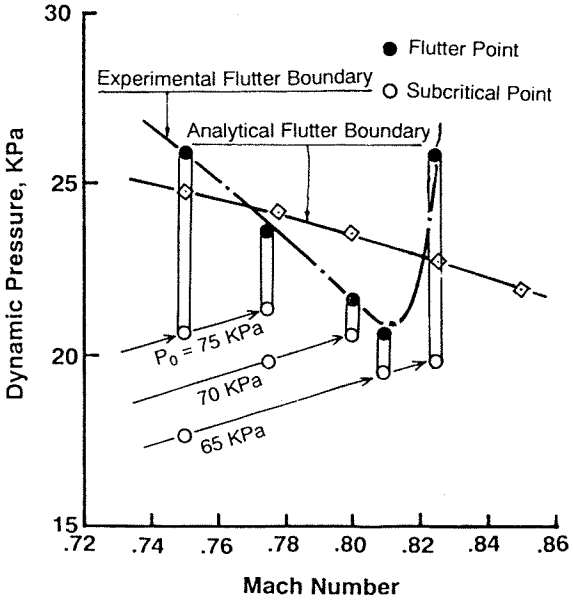


Fig. 8(a) Transonic dip phenomena

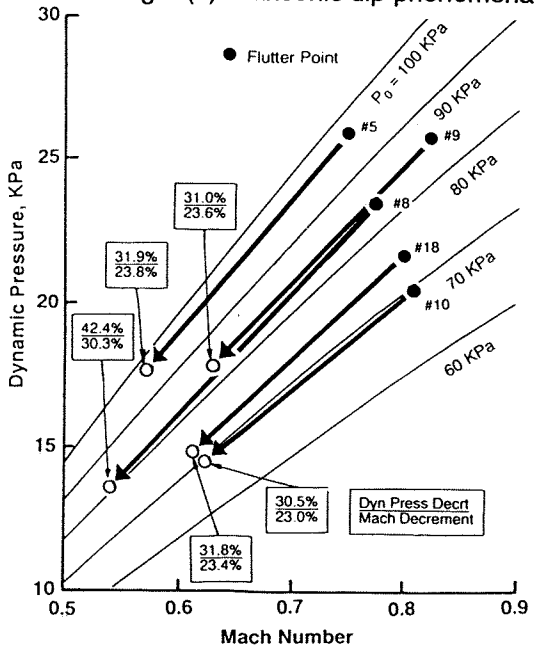


Fig. 8(b) Flutter stopper effect

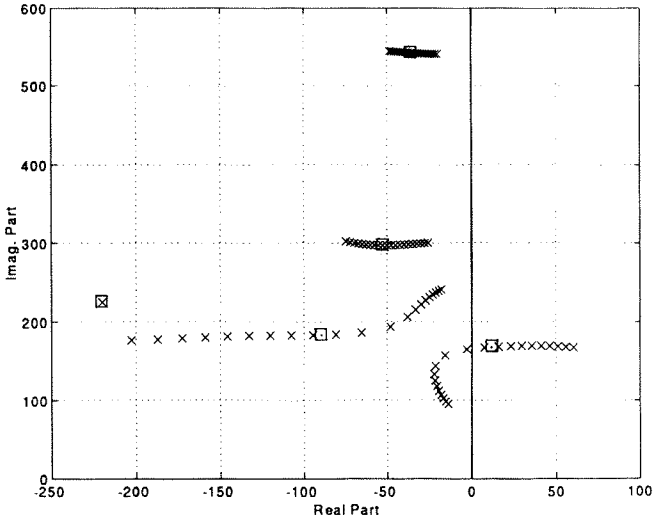


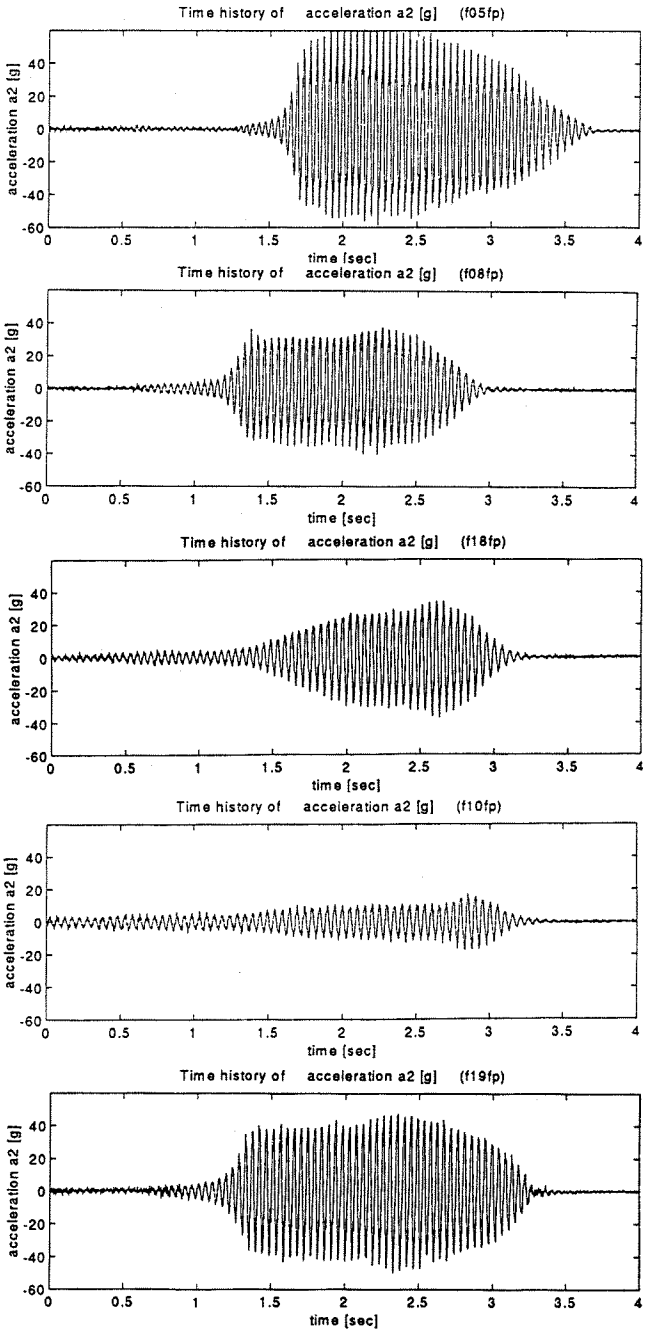


Fig. 9 Time history of limit cycle flutter.

Fig. 10 Root locus plot for a tuned math model.

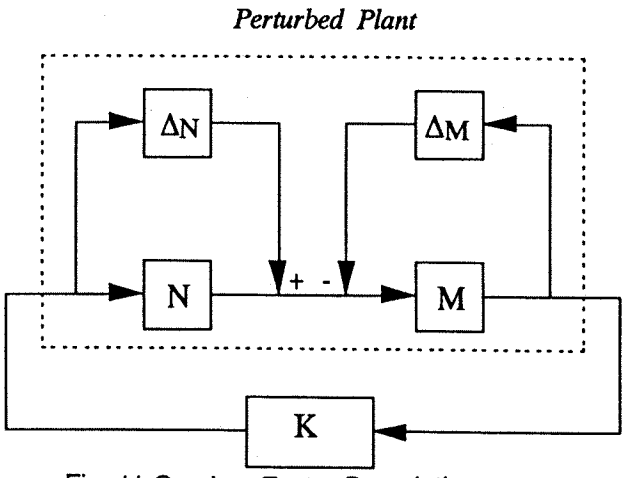


Fig. 11 Coprime Factor Description and Robust Stabilization Ploblem

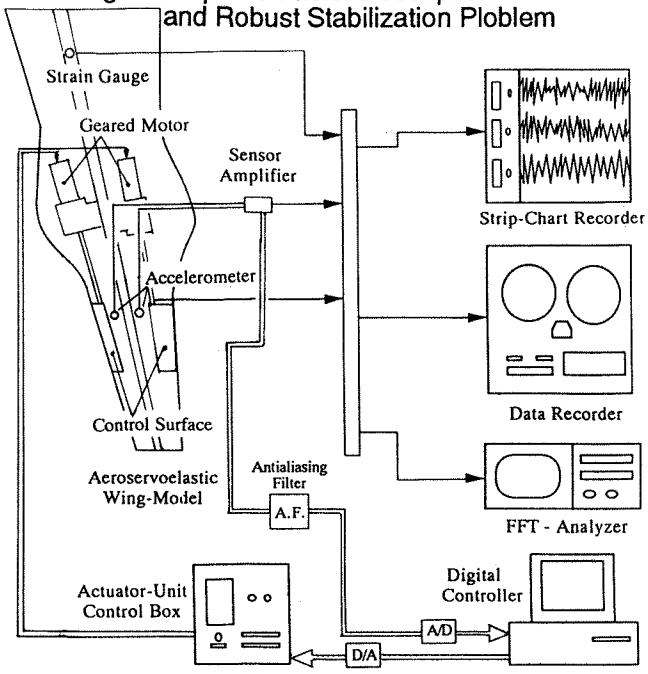


Fig. 12 A block diagram of the wind tunnel test

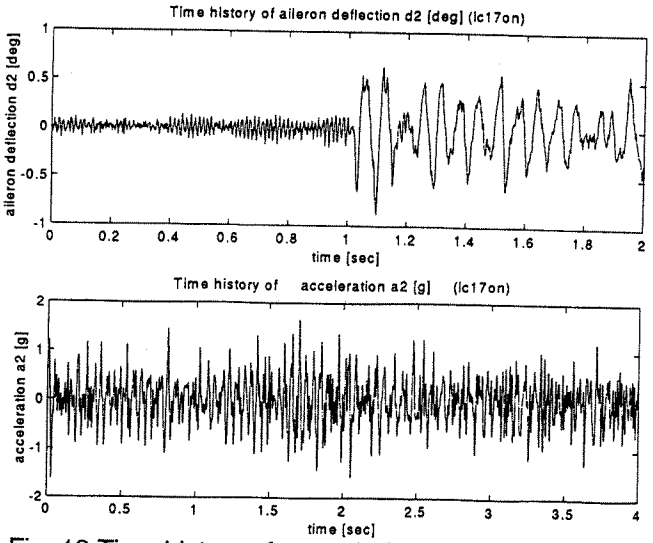


Fig. 13 Time history of control effect at subcritical condition (Control law: C2)

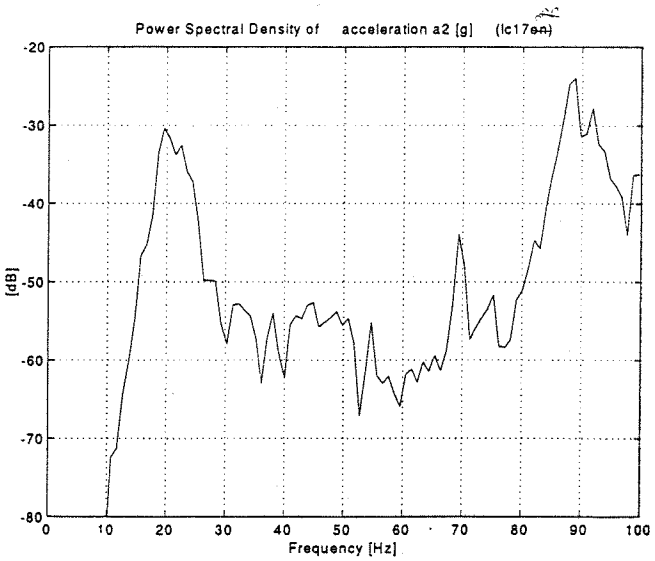


(a) Open loop

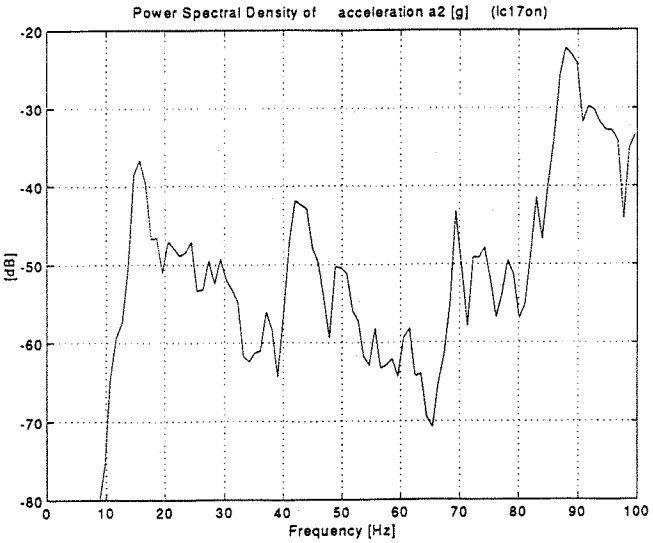


(b) Closed loop (Control law: C2)

Fig. 13 Power spectral density of acceleration response at subcritical condition